SERBIAN JOURNAL OF ELECTRICAL ENGINEERING
Vol. 18, No. 2, June 2021, 1-5

UDC: **DOI: https://doi.org/2298/SJEE**

On the Influence of Discretization Sensitivities in Time-Domain Iron Loss Estimation With the Parametric Magneto Dynamic Model

Timo Hörmann[1], Ermin Rahmanovic[2], Danilo Gartner Aurich[1], Martin Petrun[2], Simon Steentjes[1]

Abstract: Precise estimation of iron losses is crucial for advancing the design and efficiency of modern electrical machines. Given the widespread adoption of voltage-source inverters in electric drive systems, excitation waveforms often contain rich harmonic content, leading to increased and complex iron loss behavior. Simultaneously, advancements in electrical steel technology - marked by thinner laminations ($\leq 0.27\,\mathrm{mm}$), higher silicon content, and coarse grain structures - necessitate more accurate iron-loss modeling approaches. This paper utilizes the Parametric Magneto-Dynamic (PMD) model, enhanced with an inverse hysteresis formulation, to estimate iron losses in the time domain under arbitrary excitations. The proposed PMD model captures the detailed magnetization dynamics of advanced steel grades and enables a systematic investigation into how material properties - such as lamination thickness, alloy composition, and grain morphology - impact the required spatial and temporal discretization for accurate loss estimation. The paper analyzes the impact of discretization in the PMD model on both the accuracy of the iron loss prediction and the simulation time. The findings provide guidelines on the required discretization for purely sinusoidal excitation and for sinusoidal excitation with harmonic content across a range of frequencies.

Keywords: Iron loss calculation, Dynamic iron loss, Hysteresis, Electrical steel sheet, Parametric Magneto-Dynamic model.

[1]Institute of Electrical Machines, RWTH Aachen University, Aachen, Germany;
timo.hoermann@iem.rwth-aachen.de
danilo.aurich@iem.rwth-aachen.de
simon.steentjes@iem.rwth-aachen.de
[2]Faculty of Electrical Engineering and Computer Science, Institute of Electrical Power Engineering, University of Maribor, Maribor, Slovenia;
ermin.rahmanovic@um.si
martin.petrun@um.si

1 Introduction

Accurate calculation of iron losses remains a critical aspect of designing high-performance electric drives [1]. Traditional analytical models, based on statistical loss separation and sinusoidal excitation, often rely on frequency-domain techniques, such as the linear superposition of harmonic components [2], which require extensive measurement data. Approaches like [3] attempt to address non-sinusoidal excitation through separation of minor and major hysteresis loops, using DC-biased sinusoidal signals to extract parameters for models such as Bertotti's [4]. However, these frequency-domain methods are inherently unsuitable for real-time and time-domain applications. Meanwhile, advancements in electrical steel - toward thinner laminations ($\leq 0.27\,\mathrm{mm}$), higher silicon content, and coarser grain structures - introduce complexities in field distribution that are not adequately captured by conventional models.

This study addresses these limitations by employing the Parametric Magneto-Dynamic (PMD) model [5] in combination with an inverse hysteresis model to enable accurate, time-domain iron loss estimation under arbitrary excitation conditions. Unlike previous models, the PMD framework inherently supports time-domain analysis and allows for direct incorporation of nonlinear magnetization dynamics influenced by material microstructure [6, 7].

However, it is important to note that this phenomenon is strictly valid only for materials with linear magnetization behavior; in nonlinear materials, the electromagnetic field distribution may deviate significantly from classical skin effect predictions. In numerical modeling with the PMD model, the number of slices used across the thickness of a sheet material can be chosen based on both the skin depth and the characteristics of the excitation dynamics. Because skin depth governs how deeply electromagnetic fields penetrate the material, a practical rule of thumb is to assign one slice per skin depth [5] to ensure sufficient resolution in the simulation.

This work systematically analyzes the influence of sheet discretization, i.e., the selected number of slices on the accuracy and computation time of the PMD model for an iron-silicon electrical sheet. The analysis was performed under purely sinusoidal excitations as well as sinusoidal excitations with harmonic content for multiple frequencies. In addition, this work introduces a guideline for determining the adequate number of slices based on the classical skin depth for both excitation cases.

The paper is structured as follows; in section 2 a brief introduction about the PMD and used static hysteresis model is given. Section 3 gives an overview over the used material, how the measurements were executed and how the iron loss are calculated in this study. Subsequently in section 4 the results of the influence of discretization and on simulation time are presented and discussed.

2 Material Modeling Considering Major and Minor Loops

2.1 Parametric Magento-Dynamic Model

Since iron losses comprise both hysteresis and eddy current losses, it is essential to account for both, in order to accurately estimate the total iron losses in electrical sheets. The PMD model [5] is based on Maxwell's equations and enhances computational efficiency by segmenting electrical steel sheets into thinner slices and applying a piecewise approximation of magnetic quantities. This approach simplifies calculation while allowing for the integration of various static hysteresis models. The PMD model was introduced in [8], in its ability to handle arbitrary excitations was demonstrated in [6] and [7]. The PMD model, used in this study, can be expressed as

$$\vec{H}(\vec{B}) = \vec{H}_{\mathrm{sur}} - \mathbf{K}\frac{\mathrm{d}\vec{B}}{\mathrm{d}t} \tag{1}$$

where $\vec{H}(\vec{B})$ represents the averaged magnetic field strength in every slice, which depends on the flux density of the corresponding slice $\vec{H}(\vec{B}) = \left[H_1(B_1), H_2(B_2), \dots, H_{\mathrm{s}}(B_{\mathrm{s}})\right]^{\mathrm{T}}$.

Here $\vec{H}_{\mathrm{sur}} = \left[H_{\mathrm{sur}}, H_{\mathrm{sur}}, \dots, H_{\mathrm{sur}}\right]^{\mathrm{T}}$ represents the applied field strength extended uniformly to each slice, $\mathbf{K}$ is a matrix that couples the slices in the form of

$$\mathbf{K} = \sigma b_{\mathrm{s}}^2 \begin{bmatrix} (N_{\mathrm{s}}-1)+\frac{1}{3} & (N_{\mathrm{s}}-2)+\frac{1}{2} & \cdots & \frac{1}{2} \\ (N_{\mathrm{s}}-2)+\frac{1}{3} & (N_{\mathrm{s}}-2)+\frac{1}{2} & \cdots & \frac{1}{2} \\ \vdots & \vdots & \ddots & \vdots \\ \frac{1}{2} & \frac{1}{2} & \cdots & \frac{1}{3} \end{bmatrix} \tag{2}$$

with σ as the electrical conductivity and b_{s} as the thickness of each slice. b_{s} is calculated as

$$b_{\mathrm{s}} = \frac{b}{2N_{\mathrm{s}}}. \tag{3}$$

The total thickness of the sheet is denoted by b. The individual slices are indexed by $s \in N$, with $1 \le s \le N_{\mathrm{s}}$, where N_{s} denotes the total number of slices in the simulated half of the lamination. To ensure that the simulation results accurately represent the behavior of the entire sheet, a symmetric extension is applied during the evaluation phase. This process involves mirroring the computed data across the sheet's mid-plane and appropriately scaling the results to represent the full thickness b. In this context, the first slice $(s=1)$ corresponds to the mid-plane of the sheet, while the last slice $(s=N_s)$ represents the outermost layer of the simulated half. The number of slices N_s is critical in achieving high accuracy in iron loss calculations; however, increasing the N_s also results in greater computational complexity. Therefore, a balance must be found between accuracy and computational efficiency. While [9] adapted the PMD model to increase the thickness of inner slices, this paper focuses on an implementation where slices maintain a constant thickness.

The PMD model allows for simulating the magneto-dynamic behavior by current- or voltage-sources and can be coupled with external circuits, for example a finite element (FE) simulation [5]. In this case a current-driven simulation is chosen, due to its simplicity and straightforward implementation. The discretization principle is exemplarily illustrated in Fig. 1 using four slices $(N_s=4)$. The sheet's thickness is represented by b, and as Fig. 1 depicts, the innermost slice is $s=1$ and the outermost is $s=4$. By applying the PMD model, the assumption is made that the width $b \ll w$ and the length $b \ll l$.

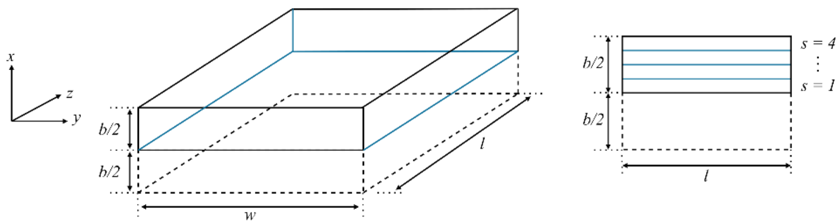

Figure 1 Schematic view of the discretization of the PMD model.

2.2 Static hysteresis model

To accurately replicate hysteresis behavior under arbitrary excitation with the PMD model, a well-suited static inverse hysteresis model is essential. Numerous hysteresis models have been developed, each with its own advantages and disadvantages, which can be found in [10]. After comparing the accuracy of several history-independent hysteresis models [11], the Tellinen (TLN) model [12] was chosen. The TLN model stands out for its ease of implementation and its ability to effectively reproduce both major and minor loops using standard measurements. The model is implemented in the form of two ordinary differential equations (ODEs)

$$\frac{\mathrm{d}H}{\mathrm{d}t} = \frac{1}{\mu_0 + \frac{B^-_{\text{major}}(H) - B}{B^-_{\text{major}}(H) - B^+_{\text{major}}(H)}\left(\frac{\mathrm{d}B^+_{\text{major}}(H)}{\mathrm{d}H} - \mu_0\right)}\frac{\mathrm{d}B}{\mathrm{d}t}, \quad \frac{\mathrm{d}B}{\mathrm{d}t} > 0 \tag{4}$$

$$\frac{\mathrm{d}H}{\mathrm{d}t} = \frac{1}{\mu_0 + \frac{B - B^+_{\text{major}}(H)}{B^-_{\text{major}}(H) - B^+_{\text{major}}(H)}\left(\frac{\mathrm{d}B^-_{\text{major}}(H)}{\mathrm{d}H} - \mu_0\right)}\frac{\mathrm{d}B}{\mathrm{d}t}, \quad \frac{\mathrm{d}B}{\mathrm{d}t} < 0 \tag{5}$$

where B^+_{major} describes the ascending and B^-_{major} the descending branch of the quasi-static BH loop of the measured material. $\mathrm{d}B^{+,-}_{\text{major}} / \mathrm{d}H$ denotes the permeability of the major loop and μ_0 the magnetic permeability constant. B is the flux density. Depending on the sign of $\mathrm{d}B / \mathrm{d}t$ the model switches between the two ODEs. In this study, the TLN model was identified using a major loop measured at $10\,\mathrm{Hz}$ with a peak flux density of $B_{\text{sat}} = 1.5\,\mathrm{T}$. The measurement were performed using a Single Sheet Tester (SST).

3 Methodology

3.1 Material specification and measurement setup

On a non-grain-oriented material, measurements, simulations, and analyses were performed. The material is a $3.2\,\mathrm{wt\%}$ non-grain-oriented electrical steel with a thickness of $b = 0.3\,\mathrm{mm}$ and dimensions of length $l = 120\,\mathrm{mm}$ and width $w = 120\,\mathrm{mm}$. The measurements required for parameterizing the TLN model and validating the PMD model were acquired using a Single Sheet Tester (SST). As discussed in Section 2.2, the TLN model was parameterized using the measured major hysteresis loop shown in Fig. 2, which serves as a look-up table embedded in the model.

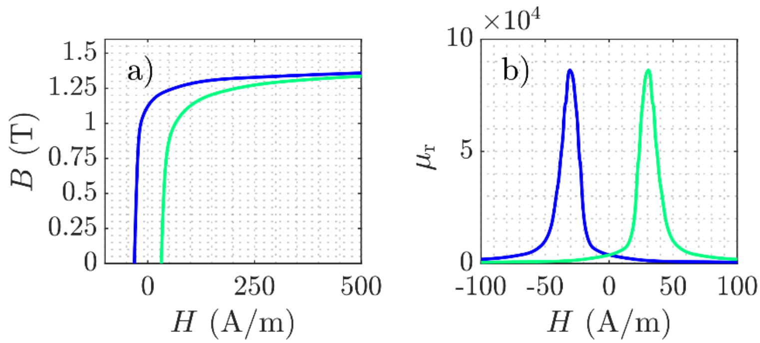

Figure 2 a) Static hysteresis loop of the electrical steel sheet used in this study; b) relative permeability μ_r derived from the major loop.

The measurements listed in Table 1 were performed and evaluated both by measurements and simulations, using different numbers of slices N_s to demonstrate the model's ability to process arbitrary excitations – in particular, purely sinusoidal and sinusoidal signals with harmonic components – using the time-based PMD model. The respective measurements are summarized in **Table 1**, where f_1 and f_3 denote the fundamental frequency and the frequency of the third harmonic of the excitation, respectively. B_1 and B_3 represent the corresponding flux densities.

Table 1

Tested excitation cases with corresponding frequencies and flux densities.

Case	Excitation
1-6	$f_1 = \{20, 100, 200, 400, 800, 1000\}$ Hz, $B_1 = 1.2$ T
7	$f_1 = 100$ Hz, $B_1 = 1.2$ T; $f_3 = 300$ Hz, $B_3 = 0.5$ T
8	$f_1 = 500$ Hz, $B_1 = 1.2$ T; $f_3 = 1500$ Hz, $B_3 = 0.5$ T

The time-dependent excitation H of a major loop, as well as that of a major loop containing minor loops, is illustrated in Fig. 3a). The corresponding time-domain waveforms of the flux density B are presented in Fig. 3b), while Fig. 3c) shows the resulting hysteresis curves. It can be observed that, at the same fundamental frequency, the presence of the harmonic component leads to a significant widening of the hysteresis curve, particularly outside the minor loops, that means, at flux densities below $0.6\,\mathrm{T}$.

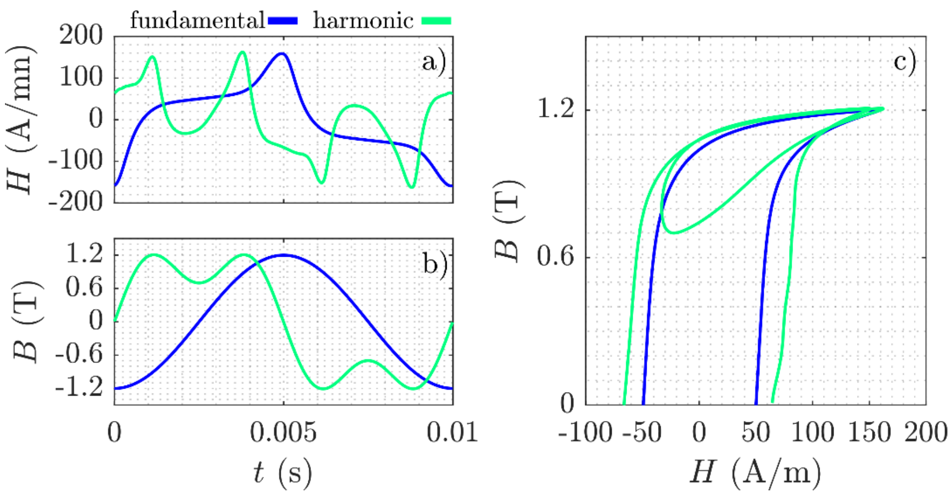

Figure 3 a) shows the time-dependent excitation H; b) shows the resulting flux densities B and c) shows the corresponding hysteresis curves,

3.2 Iron loss calculation

Iron losses play a significant role in the overall efficiency of electrical machines and accurate calculation of these losses is essential for design optimization and effective thermal management. Various methods exist for determining iron losses, depending on the type of excitation and the available data.

A widely used and physically intuitive method for determining iron losses is based on the energy dissipated per magnetic hysteresis cycle, which can be obtained from the area enclosed by the BH hysteresis loop:

$$P_\mathrm{c} = f_\mathrm{c} \oint H \,\mathrm{d}B = \frac{1}{t_\mathrm{c}} \oint H \,\mathrm{d}B \tag{6}$$

where Pc denotes the power loss due to hysteresis, f_c is the frequency and t_c the cycle time of the magnetization cycle. The classical Bertotti formula [4] describes the total iron losses as the sum of hysteresis, eddy current, and excess losses:

$$P_\mathrm{B} = c_\mathrm{hyst} B^{\alpha} f + c_\mathrm{eddy} B^2 f^2 + c_\mathrm{excess} B^{1.5} f^{1.5} \tag{7}$$

where c_hyst, c_eddy, and c_excess are material-specific parameters. The coefficient for eddy current losses can be determined by [4]:

$$c_\mathrm{eddy} = \frac{b^2 \sigma}{12}. \tag{8}$$

The remaining parameters must be identified through experiments and subsequent parameter fitting.

Since the original formulation of (7) was derived for sinusoidal excitations and requires extensive measurement data for parameter identification [2], it does not provide accurate loss predictions under arbitrary excitation waveforms. To address this limitation, a loss computation approach specifically adapted to the PMD model was proposed in [5]. This method relies solely on material data that is typically already available, significantly simplifying its practical application. The power loss per slice due to eddy currents, $P_\mathrm{ec,s}$, is given by:

$$P_\mathrm{ec,s} = f_\mathrm{c} \int_{t_\mathrm{s}}^{t_\mathrm{e}} \left[\frac{\sigma b_\mathrm{s}^2}{N_\mathrm{s} \rho} \left(\left(\sum_{i=1}^{s-1} \frac{\mathrm{d}B_i}{\mathrm{d}t} \right)^2 + \left(\sum_{i=1}^{s-1} \frac{\mathrm{d}B_i}{\mathrm{d}t} \right) \frac{\mathrm{d}B_\mathrm{s}}{\mathrm{d}t} + \frac{1}{3} \left(\frac{\mathrm{d}B_\mathrm{s}}{\mathrm{d}t} \right)^2 \right) \right] \mathrm{d}t \tag{9}$$

here, t_s and t_e denote the start and end times of the magnetization cycle, respectively, and B_s represents the flux density in the respective slice s. To obtain the total eddy current-induced iron loss, P_ec, the slice-wise contributions from (9) must be summed over all slices:

$$P_{\mathrm{ec}} = \sum_{i=1}^{N_{\mathrm{s}}} P_{\mathrm{ec},i}. \tag{10}$$

The hysteresis losses per slice, $P_{\mathrm{hyst,s}}$, are calculated by:

$$P_{\mathrm{hyst,s}} = f_{\mathrm{c}} \int_{t_{\mathrm{s}}}^{t_{\mathrm{e}}} \frac{1}{N_{\mathrm{s}}\rho} H_{\mathrm{s}} \frac{\mathrm{d}B_{\mathrm{s}}}{\mathrm{d}t} \mathrm{d}t, \tag{11}$$

to obtain the total hysteresis loss, P_{hyst}, the individual slice contributions must be summed in the same manner as in (10). To compare the measured iron losses with those predicted by the PMD model, the total power loss per cycle, $P_{\mathrm{c,n}}$, is determined by summing (10) and (11):

$$P_{\mathrm{c,n}} = P_{\mathrm{ec}} + P_{\mathrm{hyst}}. \tag{12}$$

To validate the simulation results, both absolute and relative errors are used. The absolute error is defined as

$$\epsilon_{\mathrm{a}} = P_{\mathrm{m}} - P_{\mathrm{c,n}} \tag{13}$$

And the relative error as

$$\epsilon_{\mathrm{r}} = \frac{P_{\mathrm{m}} - P_{\mathrm{c,n}}}{P_{\mathrm{m}}} \cdot 100\,\%. \tag{14}$$

The absolute error (13) and relative error (14), alongside (10) and (11), are used as metrics in the present study to assess the accuracy of the PMD model under various excitation conditions.

4 Results

Since this study investigates the influence of slice count on simulation time, all simulations were conducted on identical hardware to ensure consistent conditions. Both the PMD model and the implemented TLN model were developed in MATLAB/Simulink. Consequently, the choice of the numerical solver and its settings directly affect the simulation results.

In this work, the built-in MATLAB solver ode23tb was employed with a variable step size, which was limited to a maximum step size of $1 \cdot 10^{-3}$ s. Both the relative and absolute error tolerances were set to $5 \cdot 10^{-8}$ s, ensuring a balance between accuracy and computational efficiency.

Each simulation was run for 10 consecutive cycles, as the PMD model requires several cycles—depending on the material properties—to reach a stable steady-state behaviour. For the purpose of analysis, only the results from the last cycle were considered.

4.1 Spatial behaviour

Since (7) assumes a homogeneous field distribution within the material [4], it does not accurately capture the non-uniform field behavior illustrated in Fig. 4, resulting in imprecise iron loss estimations. Unlike the approach in [5], which specifically addresses field distribution under viscous magnetic conditions, this study does not consider magnetic viscosity.

As illustrated in Fig. 4a), the magnetic field distribution within the sheet is already non-uniform at $100\ \mathrm{Hz}$ and exhibits a phase lag, as the inner slices reach the applied flux density later in time. This behavior highlights the necessity of discretizing the electrical steel sheet—an approach inherently provided by the PMD model. The following time-dependent figures were normalized by magnetization cycle time t_c, whereas the spatial-dependent figure are normalized by the sheets thickness b.

The simulation results also show field attenuation within the material: the innermost slice (depicted in vibrant blue) exhibits significantly lower flux density compared to the outermost slice (shown in light green) at $t/t_\mathrm{c} = 0.25$. Fig. 4b) and d) shows the flux density averaged across all slices over slice position. As expected, the field distribution remains nearly homogeneous at $t/t_\mathrm{c} = 0.0$ and $t/t_\mathrm{c} = 0.5$, while the most significant variation across the sheet occurs around $t/t_\mathrm{c} \approx 0.2$.

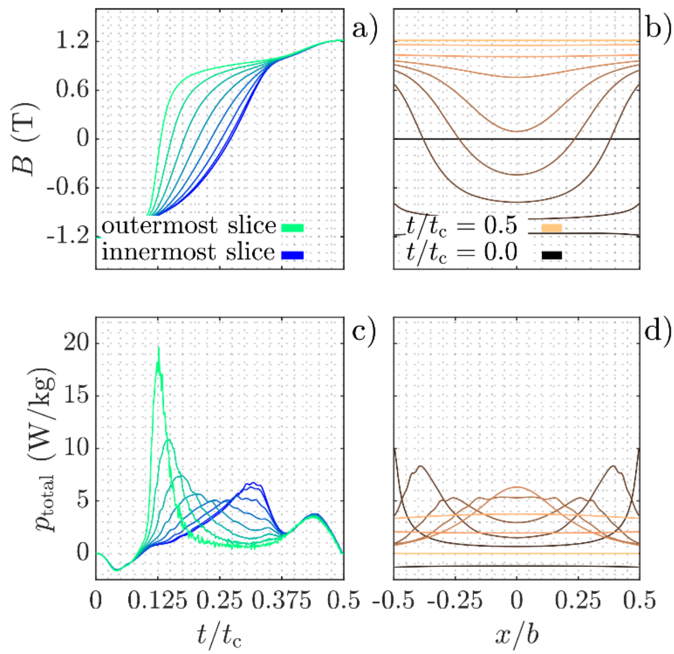

Figure 4 Simulation results at an excitation frequency of 100 Hz *and a peak flux density of* 1.2 T *. (a) Flux density distribution over time, (b) Flux density distribution across sheet positions, (c) Total power loss* p_{total} *over time, (d) Total power loss across sheet positions.*

In Fig. 5, the field distribution at 400 Hz is shown. At this higher frequency, the disparity between the innermost and outermost slices increases further, reinforcing the importance of spatially resolved modeling for accurate representation of the internal field behavior. Also there occurs a transient power peak due to high $\mathrm{d}B/\mathrm{d}t$ as shown in Fig. 5c).

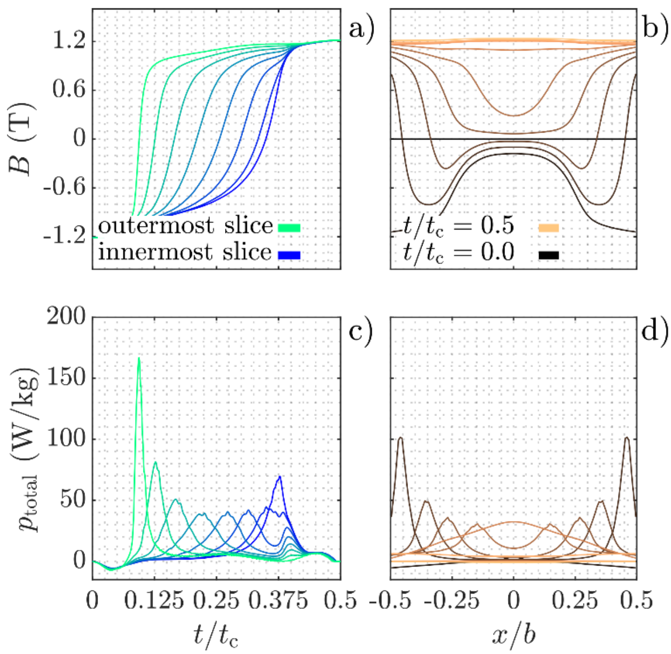

Figure 5 Simulation results at an excitation frequency of 400 Hz *and a peak flux density of* 1.2 T *. (a) Flux density distribution over time, (b) Flux density distribution across sheet positions, (c) Total power loss* p_{total} *over time, (d) Total power loss across sheet positions.*

At higher excitation frequencies, such as 1000 Hz, the variation in field distribution becomes even more pronounced, as shown in Fig. 6. The outermost slice exhibits a behavior characteristic of the well-known hysteresis loop, whereas the innermost slice shows a smoother and more delayed response over time. The outermost slice exhibits a high power in a short time (up to 650 W/kg), whereas the inner slices exhibit much lower power levels ($\approx$ 250 W/kg). The instantaneous power of the slices exhibits wave-like behavior, with the peak propagating from one slice to the next toward the interior of the sheet with a time delay. This phenomenon can be observed at lower frequencies as well, but it is less distinctly expressed.

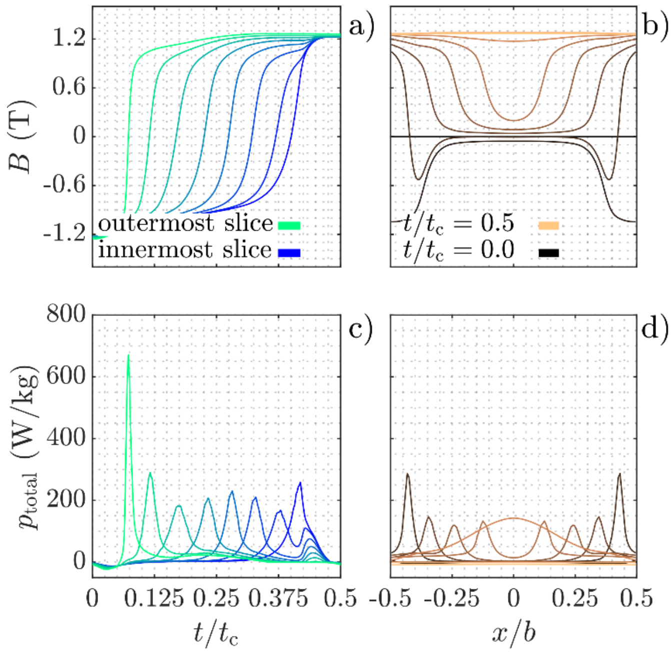

Figure 6 a) shows the flux density distribution over time at an excitation frequency of 1000 Hz *and a peak flux density of* 1.2 T *, while b) presents the flux density distribution across the sheet position. c) and d) illustrates the total power loss* p_{total} *over time and slice position, respectively.*

In Fig. 7, a non-sinusoidal excitation is applied, consisting of a fundamental component with an amplitude of 1.2 T at 100 Hz and a third-order harmonic with an amplitude of 0.5 T. A phase lag is observed in the inner slices. At $t = 0.0$, the flux density distribution resembles that of pure sinusoidal excitation. However, when the harmonic component becomes significant ($t \approx 0.2$), the flux density in the inner slices decreases, even falling below the excitation level.

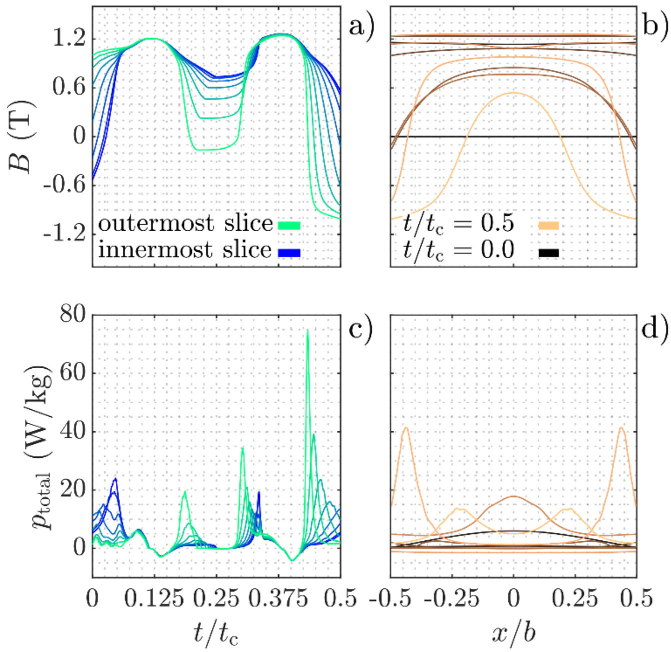

Figure 7 a) shows the flux density distribution over time at an excitation frequency of 100 Hz *and a peak flux density of* 1.2 T *, including a harmonic component at* 300 Hz *with an amplitude of* 0.5 T *. b) presents the flux density distribution across the sheet position. c) and d) illustrates the total power loss* p_{total} *over time and sheet position, respectively.*

By increasing the fundamental frequency from 100 Hz to 500 Hz, the outermost slice exhibits a flux density of approximately -1.0 T, at $t \approx 0.2$ indicating that the harmonic component of the excitation causes a flux inversion in the outer regions of the electrical steel sheets, as shown in Fig. 8.

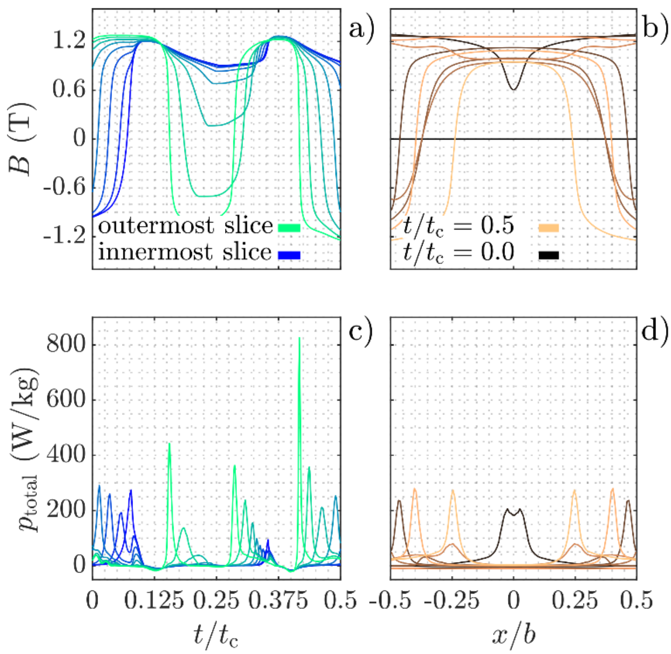

Figure 8 a) shows the flux density distribution over time at an excitation frequency of 500 Hz *and a peak flux density of* 1.2 T *, including a harmonic component at* 1500 Hz *with an amplitude of* 0.5 T *. b) presents the flux density distribution across the sheet position. c) and d) illustrates the total power loss* p_{total} *over time and sheet position, respectively.*

4.2 Influence of discretization on accuracy and simulation time

As shown in Section 4.1, selecting an appropriate number of slices is essential to accurately capture the inhomogeneous flux distribution caused by eddy currents. First, the influence of the slice count N_s on the simulation time t_{sim} is investigated. As illustrated in Fig. 9, the simulation time decreases with increasing frequency. At frequencies above 100 Hz, the simulation time reliably converges to a frequency-independent value across all tested values.

Furthermore, depending on the excitation frequency, increasing the number of slices N_s does not necessarily lead to improved accuracy. This suggests that, beyond a certain point, additional discretization does not lead to greater accuracy.

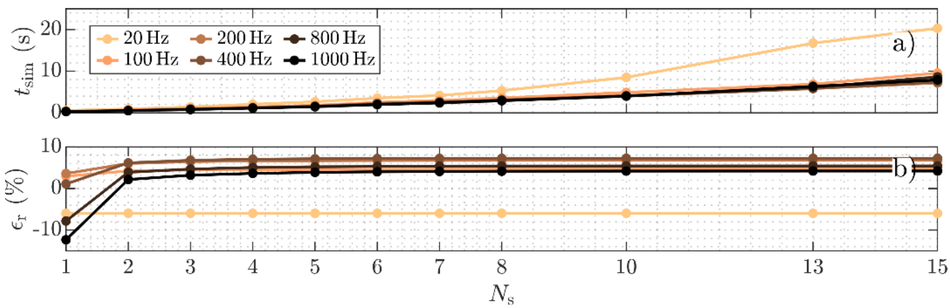

Figure 9 Simulation time t_{sim} and relative error versus N_{s} for fundamental excitations.

This is further confirmed by the simulation results under harmonic excitation, as shown in Fig. 10. The simulation time is approximately $t_{\mathrm{sim}} = 20\,\mathrm{s}$, which is slightly higher compared to the simulation with a $100\,\mathrm{Hz}$ fundamental excitation. The relative error ϵ_{r} converges for the $500\,\mathrm{Hz}$ simulation when the number of slices reaches $N_{\mathrm{s}} = 8$.

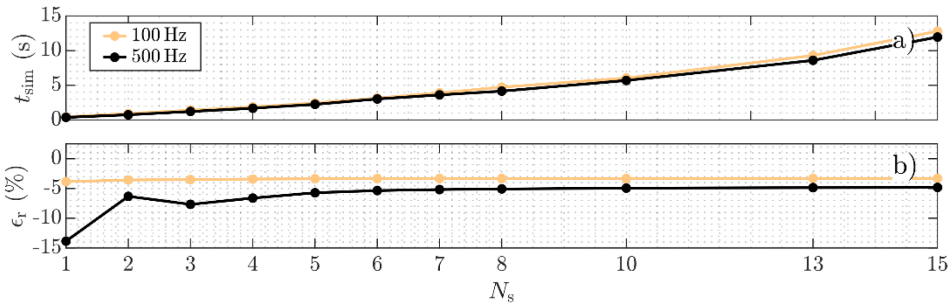

Figure 10 Simulation time t_{sim} and relative error versus N_{s} for harmonic excitations.

Fig. 11 provides an overview of the power losses due to eddy currents (P_{ec}), hysteresis losses (P_{hyst}), and the total losses (P_{total}). Additionally, the absolute error (ϵ_{a}) and the relative error (ϵ_{r}) are shown. Figs. 11a), c), e), g), and i) illustrate the frequency dependency, while Figs. 11b), d), f), h), and j) display the slice-dependent values. This enables a more detailed analysis of the model behavior. The red dots in Figs. 11e) and f) indicate the total measured iron losses from the experiments.

Fig. 11a) confirms the expected quadratic increase of eddy current losses with frequency, while the hysteresis losses P_{hyst} increase approximately linearly. Furthermore, it can be observed that the hysteresis losses are consistently lower than the eddy current losses. The total losses P_{total} show good overall agreement with the measured losses P_{m}.

As illustrated in Fig. 11i), the PMD model tends to overestimate losses at low frequencies and underestimate them at mid-range frequencies. This deviation may result from the absence of additional effects—such as viscous fields—and the fact that the TLN model parametrization was based on measurements at $10\,\mathrm{Hz}$, which is not a truly static measurement. At higher frequencies, the estimation becomes more accurate again, except when only a single slice ($N_s = 1$) is used for discretization.

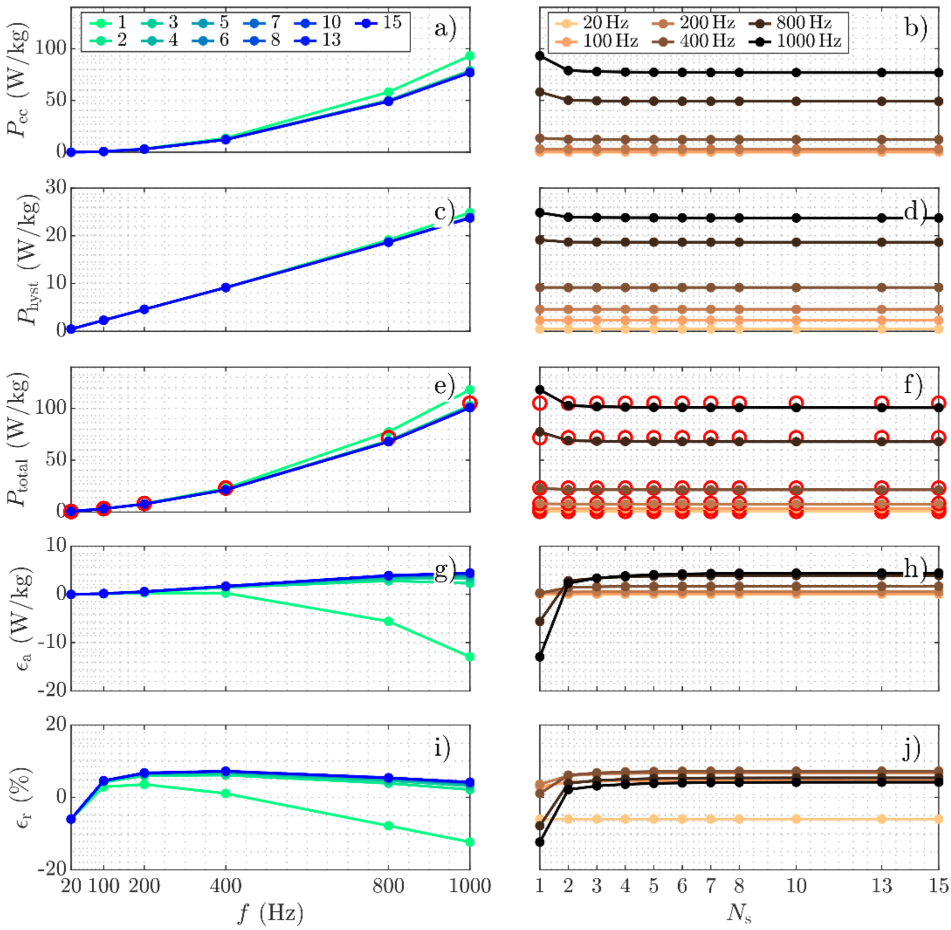

Figure 11 Time- and slice-count-dependent power loss components with relative and absolute errors at fundamental excitation.

The simulation results for harmonic excitation are shown in Fig. 12. The red bars represent the measured total iron losses P_m at $f_1 = 100\,\mathrm{Hz}$ and $f_1 = 500\,\mathrm{Hz}$. As previously described, the excitation consists of a fundamental frequency component f_1 and a third-order harmonic. The amplitude of the fundamental component is set to $1.2\,\mathrm{T}$, while the third harmonic is set to $0.5\,\mathrm{T}$.

At $f_1 = 100\,\mathrm{Hz}$, the PMD model provides an accurate iron loss estimation with as few as $N_s = 6$ slices. When using $N_s = 10$, the model accurately replicates the magnetic behavior across the sheet.

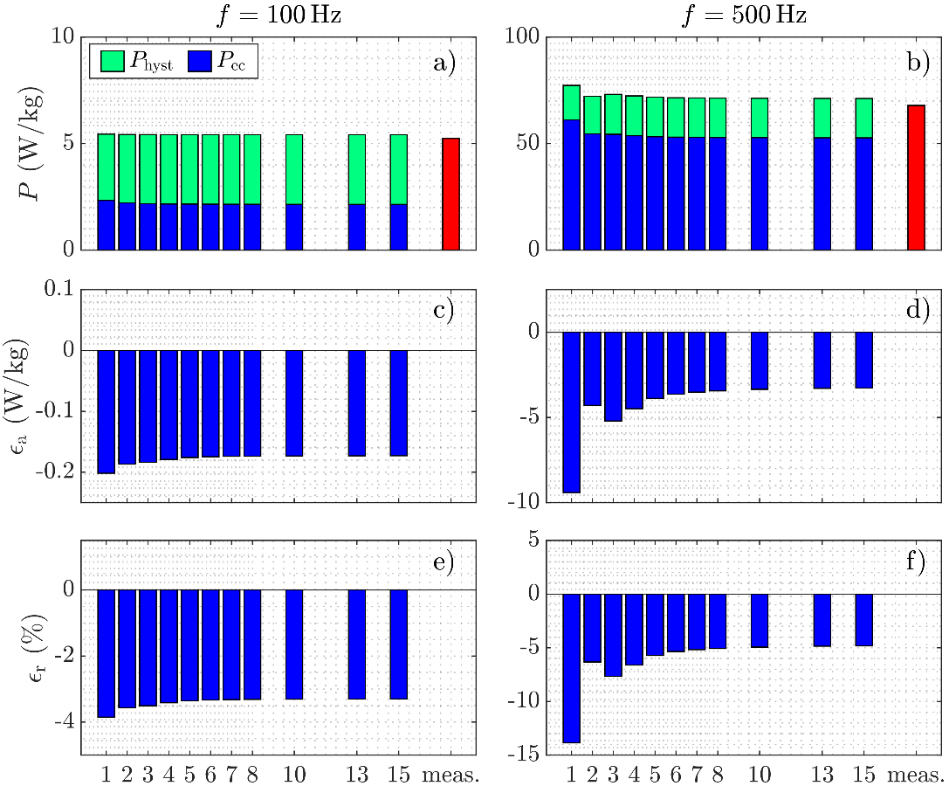

Figure 12 Slice-count-dependent power loss components with relative and absolute errors at harmonic excitation.

The total power loss P_{total}, as well as the separated eddy current losses P_{ec} and hysteresis losses P_{hyst} as a function of the slice count N_s, are shown in Figs. 13a), b), and c). The red dots in Fig. 13c) represent the experimentally measured losses. A relative error of only $5\,\%$ is achieved using the PMD model when the slice count reaches $N_s \geq 10$.

In comparison to Fig. 11, the PMD model tends to overestimate the losses under harmonic excitation.

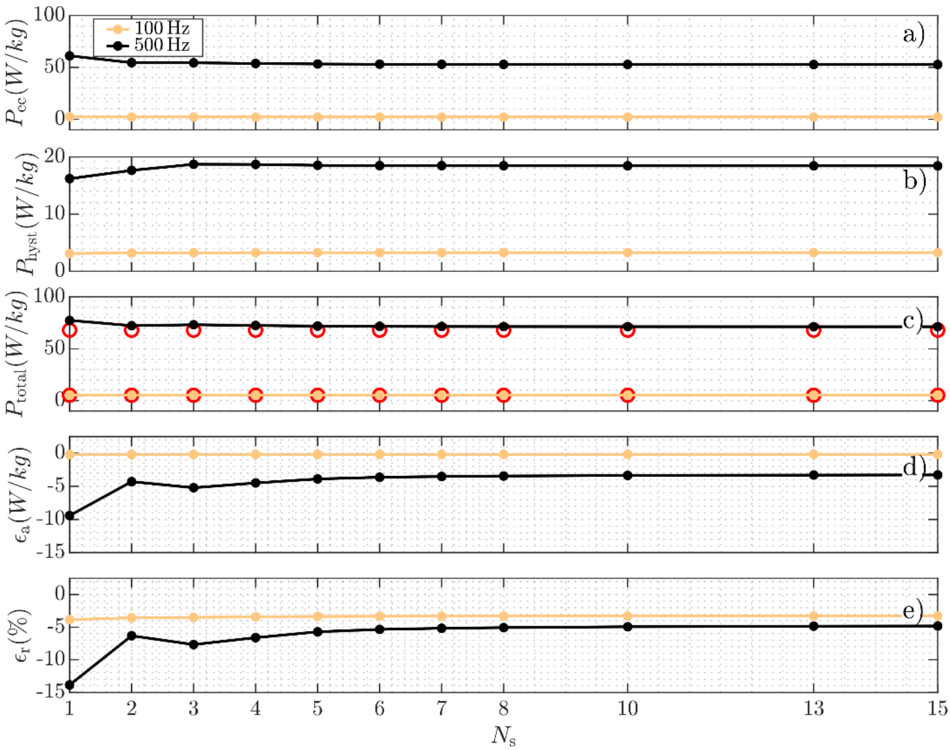

Figure 13 Time-count-dependent power loss components with relative and absolute errors at harmonic excitation.

4.3 Derivation of a rule of thumb for discretization

As previously mentioned in [5], discretization was chosen such that one slice was applied per skin depth. When no eddy currents are present in the material, or when the skin depth exceeds the sheet thickness, a single slice is sufficient, as the magnetic field distribution remains approximately homogeneous. However, as stated in Section 4.1, this assumption already fails at relatively low frequencies around 100 Hz . For arbitrary excitations, the assumption of a homogeneous field is also invalid. Therefore, this paper introduces a rule of thumb to estimate the minimum number of slices required to accurately model the field distribution in electrical steel sheets using the PMD model under sinusoidal as well as under non-sinusoidal excitation.

The minimum skin depth $\delta_{\min}$ is calculated by

$$\delta_{\min} = \sqrt{\frac{1}{\pi f_{\max} \mu_0 \mu_{\mathrm{r,max}} \sigma}}, \tag{15}$$

where fmax is the highest occurring excitation frequency, μ_0 is the vacuum permeability and σ is the electrical conductivity. The maximum relative permeability $\mu_{\mathrm{r,max}}$ of the investigated steel sheet, is determined by

$$\mu_{\mathrm{r,max}} = \frac{1}{\mu_0} \max\left(\frac{\mathrm{d}B}{\mathrm{d}H}\right). \tag{16}$$

The number of slices N_s is then determined by

$$N_\mathrm{s} = \left\lceil \frac{b}{\delta_{\min}} \right\rceil \tag{17}$$

where b is the sheet thickness. The ceiling function ensures complete coverage of the inhomogeneous field distribution.

Table 2 compares the analytically calculated and graphically determined slice counts for various excitation frequencies. The results confirm that the proposed rule of thumb is applicable for both purely sinusoidal excitations and those containing harmonic components, provided the respective maximum values are used.

Table 2

Calculated and graphically determined number of slices N_s and skin depths for the fundamental and harmonic frequencies.

Excitation frequency [Hz]	20	100	200	400	800	1000
	1	3	4	5	8	8
	2	3	4	5	7	8

Excitation frequency [Hz]	$300\,(100 \cdot 3)$	$1500\,(500 \cdot 3)$
	6	10
	5	10

5 Conclusion and Outlook

This paper examined the application of the PMD model coupled with the static hysteresis TLN model to a non-grain oriented electrical steel grade. The results highlight the necessity of accurately estimating both hysteresis and eddy current losses in order to improve loss prediction in electrical machines. By incorporating the PMD model, the magnetization behavior across the thickness of the material can be resolved, offering valuable insights into flux density distribution and magneto dynamic effects.

The PMD model's piecewise approximation simplifies the numerical treatment of eddy currents while allowing for spatial resolution across the sheet. However, a trade-off emerges between simulation accuracy and computational effort, directly influenced by the chosen number of slices. To address this, a skin-depth-based rule of thumb was introduced, enabling accurate estimation of the required number of slices even for arbitrary excitations with harmonic content, without unnecessarily increasing the simulation time. This approach was validated against simulation and experimental data, demonstrating reliable performance when the maximum expected frequency and relative permeability are used in the calculation.

It has also been shown that the PMD model inherently captures the inhomogeneous behavior of the magnetic field, especially in the case of high-frequency and harmonic excitation, where significant attenuation and phase delay occur within the material. This leads to a more accurate time-domain-based estimation of iron losses with less measurement effort compared to Bertotti's model, as only the major hysteresis loop, electrical conductivity, and material dimensions are required.

Future work will focus on validating the proposed rule of thumb for slice count selection under more complex excitation patterns, such as those encountered in PWM-driven systems. Additionally, the PMD model will be investigated for a broader set of electrical steel materials and under a wider range of excitation waveforms. This will allow assessment of the model's robustness and extend its applicability to real-world power electronic and electric machine applications.

6 References

[1] G. Mörée, M. Leijon: Iron loss models: A review of simplified models of magnetization losses in electrical machines, Journal of Magnetism and Magnetic Materials, vol. 609, p. 172163, 2024.

[2] S. Steentjes, G. von Pfingsten, M. Hombitzer, K. Hameyer: Iron-Loss Model With Consideration of Minor Loops Applied to FE-Simulations of Electrical Machines, IEEE Transactions on Magnetics, vol. 49, pp. 3945–3948, July 2013.

[3] T. Taitoda, Y. Takahashi, K. Fujiwara: Iron Loss Estimation Method for a General Hysteresis Loop With Minor Loops, IEEE Transactions on Magnetics, vol. 51, pp. 1–4, Nov. 2015.

[4] G. Bertotti: Hysteresis in magnetism. Academic Press series in electromagnetism, San Diego, Calif. [u.a.]: Academic Press, 1998. Includes bibliographical references.

[5] M. Petrun, S. Steentjes: Iron-Loss and Magnetization Dynamics in Non-Oriented Electrical Steel: 1-D Excitations Up to High Frequencies, IEEE Access, vol. 8, pp. 4568–4593, 2020.

[6] M. Petrun, S. Steentjes, K. Hameyer, D. Dolinar: 1-D Lamination Models for Calculating the Magnetization Dynamics in Non-Oriented Soft Magnetic Steel Sheets, IEEE Transactions on Magnetics, vol. 52, pp. 1–4, Mar. 2016.

[7] M. Petrun, S. Steentjes, K. Hameyer, D. Dolinar: Magnetization Dynamics and Power Loss Calculation in NO Soft Magnetic Steel Sheets Under Arbitrary Excitation, IEEE Transactions on Magnetics, vol. 51, pp. 1–4, Jan. 2015.

[8] M. Petrun, V. Podlogar, S. Steentjes, K. Hameyer, D. Dolinar: A Parametric Magneto-Dynamic Model of Soft Magnetic Steel Sheets, IEEE Transactions on Magnetics, vol. 50, pp. 1–4, Apr. 2014.

[9] L. Chen, Z. Zhang, T. Ben, H. Zhao: Dynamic Magnetic Hysteresis Modeling Based on Improved Parametric Magneto-Dynamic Model, IEEE Transactions on Applied Superconductivity, vol. 32, pp. 1–5, Sept. 2022.

[10] G. Mörée, M. Leijon: Review of hysteresis models for magnetic materials, Energies, vol. 16, no. 9, 2023.

[11] S. Steentjes, K. Hameyer, D. Dolinar, M. Petrun: Iron-Loss and Magnetic Hysteresis Under Arbitrary Waveforms in NO Electrical Steel: A Comparative Study of Hysteresis Models, IEEE Transactions on Industrial Electronics, vol. 64, pp. 2511–2521, Mar. 2017.

[12] J. Tellinen: A simple scalar model for magnetic hysteresis, IEEE Transactions on Magnetics, vol. 34, pp. 2200–2206, July 1998.